Supplementary Information for

A palette of rechargeable mechanoluminescent fluids produced by a biomineral-inspired suppressed dissolution approach

Fan Yang[1,2,3], Xiang Wu[1,2,3], Han Cui[1,2,3], Shan Jiang[1,2], Zihao Ou[1,2], Sa Cai[1,2] and Guosong Hong[1,2,*]

[1] Department of Materials Science and Engineering, Stanford University, Stanford, CA, 94305, USA
[2] Wu Tsai Neurosciences Institute, Stanford University, Stanford, CA, 94305, USA
[3] These authors contributed equally to this work.
[*] Corresponding author: guosongh@stanford.edu

This PDF file includes:

Materials and Methods

Synthesis of $Sr_2MgSi_2O_7$:Eu,Dy bulk mechanoluminescent (ML) phosphor and colloidal nanocrystals.

$Sr_2MgSi_2O_7$:Eu,Dy bulk ML phosphor was synthesized via a solid state reaction. Briefly, 2332.56 mg of $SrCO_3$ (15.8 mmol), 961.28 mg of SiO_2 (16 mmol), 777.04 mg of $(MgCO_3)_4 \cdot Mg(OH)_2 \cdot 5H_2O$ (1.6 mmol), 8.4 mg of Eu_2O_3 (0.024 mmol), 29.84 mg of Dy_2O_3 (0.08 mmol), and 29.66 mg of H_3BO_3 (0.48 mmol) were ground for 1 h and then annealed at 1050 °C for 2 h under 5% H_2 in Ar. The as-prepared $Sr_2MgSi_2O_7$:Eu,Dy bulk ML phosphor was ball-milled using a high energy ball mill for 30 min to yield slightly smaller bulk particles to prepare for the suppressed dissolution process. In the suppressed dissolution process , 2000 mg of ball-milled $Sr_2MgSi_2O_7$:Eu,Dy phosphor were added into 240 mL of sodium citrate buffer (0.08 mol/L, pH=6) and stirred at 80 °C for 72 h. Finally, $Sr_2MgSi_2O_7$:Eu,Dy colloidal nanocrystals were obtained by centrifugation at 1000 rpm for 10 min to remove large $Sr_2MgSi_2O_7$:Eu,Dy particles.

Synthesis of ZnS:Cu,Al bulk ML phosphor and colloidal nanocrystals.

ZnS:Cu,Al bulk ML phosphor was synthesized via a solid state reaction. First, 5.24 mg of copper acetylacetonate (0.02 mmol) was dissolved in 2 mL of chloroform to prepare a copper stock solution (0.01 mol/L). Additionally, 1960 mg of ZnS (20 mmol), 6 mg of Al_2O_3 (0.06 mmol), and 12 mg of H_3BO_3 were weighed and added into an agate mortar. In the meantime, 20 µL of the copper stock solution was added into the agate mortar and ground for 1 h. Finally, The mixture was annealed at 1100 °C for 2 h under 5% H_2 in Ar. After cooling down to room temperature, the as-prepared ZnS:Cu,Al bulk ML phosphor was ball-milled using a high energy ball mill for 30 min. The same suppressed dissolution procedure used for preparation of $Sr_2MgSi_2O_7$:Eu,Dy colloidal nanocrystals was followed to synthesize ZnS:Cu,Al colloidal nanocrystals.

Synthesis of ZnS:Mn bulk ML phosphor and colloidal nanocrystals.

ZnS:Mn bulk phosphor was synthesized via a solid state reaction. Specifically, 1960 mg of ZnS (20 mmol), 2.3 mg of $MnCO_3$ (0.02 mmol), and 12 mg of H_3BO_3 were ground in an agate mortar for 1 h and then annealed at 1100 °C for 2 h under 5% H_2 in Ar. After cooling down to room temperature, the as-prepared ZnS:Mn bulk ML phosphor was ball-milled using a high energy ball mill for 30 min. The same suppressed dissolution procedure used for preparation of $Sr_2MgSi_2O_7$:Eu,Dy colloidal nanocrystals was followed to synthesize ZnS:Mn colloidal nanocrystals.

Synthesis of $CaTiO_3$:Pr ML phosphor and colloidal nanocrystals.

$CaTiO_3$:Pr bulk phosphor was synthesized via a solid state reaction. Specifically, 1000 mg of $CaCO_3$ (10 mmol), 800 mg of TiO_2 (10 mmol), and 49 mg of Pr_2O_3 (0.15 mmol)

were ground in an agate mortar for 1 h and then annealed at 1300 °C for 2 h in air. After cooling down to room temperature, the as-prepared $CaTiO_3$:Pr bulk ML phosphor was ball-milled using a high energy ball mill for 30 mins. The same suppressed dissolution procedure used for preparation of $Sr_2MgSi_2O_7$:Eu,Dy colloidal nanocrystals was followed to synthesize $CaTiO_3$:Pr colloidal nanocrystals.

PEGylation of $Sr_2MgSi_2O_7$:Eu,Dy ML colloidal nanocrystals.
First, $Sr_2MgSi_2O_7$:Eu,Dy colloids were dialyzed in a cellulose dialysis tubing (molecular weight cutoff = 30 kDa) for 2 days. 40 µL of sodium hydroxide solution (10 mol/L) was then added into 20 mL of the $Sr_2MgSi_2O_7$:Eu,Dy colloidal solution (6 mg/mL) and sonicated for 1 h at room temperature. Subsequently, the $Sr_2MgSi_2O_7$:Eu,Dy colloids were washed with water and anhydrous DMF three times in each solvent and then dispersed in DMF. 40 mg of mPEG-silane (20 kDa) was added into 10 mL of the $Sr_2MgSi_2O_7$:Eu,Dy colloids in DMF and sonicated at 50 °C for 4 h. Finally, the PEGylated-$Sr_2MgSi_2O_7$:Eu,Dy colloids were washed with anhydrous DMF and water three times in each solvent and then dispersed in water for colloidal stability assessment and *in vivo* experiments.

Structure and morphology characterizations. X-ray diffraction (XRD) patterns of all bulk ML phosphors and suppressed dissolution-produced colloidal nanocrystals were acquired via a diffractometer (PANalytical Empyrean, Malvern Panalytical Ltd., Malvern, United Kingdom). Scanning electron microscope (SEM) images of all bulk ML phosphors were captured by an Apreo S LoVac SEM (Thermo Fisher Scientific, Waltham, MA). The transmission electron microscope (TEM) images of all suppressed dissolution-produced colloidal nanocrystals were recorded by a Tecnai TEM (FEI Company, Hillsboro, OR). The hydrodynamic diameter and zeta potential of bulk ML particles and ML colloids were characterized by a NanoBrook Omni dynamic light scattering (DLS) instrument (Brookhaven Instruments, Holtsville, NY).

Colloidal stability assessment. $Sr_2MgSi_2O_7$:Eu,Dy bulk particles, citrate-capped colloids, and PEGylated colloids were suspended in water or fetal bovine serum (FBS). The suspensions were charged by a 365-nm LED at 0.13 mW/mm^2 for 5 s. The bright-field and luminescence images were acquired using a digital complementary metal-oxide semiconductor (CMOS) camera (ORCA-Flash 4.0, Hamamatsu Photonics, Hamamatsu City, Japan). To assess the chronic stability of ML bulk particles and colloids, the same imaging procedure was carried out every day for 7 days.

Optical characterizations. The photoluminescence excitation and emission spectra of all bulk ML phosphors and suppressed dissolution-produced colloidal nanocrystals were measured by a Horiba FluoroLog Fluorometer. The mechanoluminescence spectra were

measured by mixing and curing bulk ML phosphors and colloidal nanocrystals in a polydimethylsiloxane (PDMS) phantom with a concentration of 70 mg/ml for all ML materials. Specifically, the PDMS phantom with ML materials was placed at the focus of an focused ultrasound (FUS) transducer with a central frequency of 1.5 MHz and charged by a 365-nm UV light emitting diode (LED; SOLIS-365C, Thorlabs, Newton, NJ) with a power density of 0.5 mW/mm^2. After 10 s of charging, FUS pulses with a repetition rate of 1 Hz were immediately applied. Meanwhile, the mechanoluminescence spectra was collected by a fiber-coupled OCEAN-HDX-VIS-NIR spectrometer (Ocean Insight, Orlando, FL). Averaging over multiple measurements was applied to reduce the noise of the mechanoluminescence spectrum. In addition, the thermoluminescence (TL) spectra were acquired by a SL-08 TL reader (Guangzhou Radiation Science and Technology, Guangzhou, China) with a heating rate of 2 °C/s from room temperature to 280 °C.

Constant composition (CC) technique. The overall dissolution flux of all ML crystals was measured by following a previously reported protocol.[1] Specifically, undersaturated solutions (30 mL) were prepared by adding 180 μL of $SrCl_2$ (1 mol/L) and 90 μL of $MgCl_2$ (1 mol/L) solutions for $Sr_2MgSi_2O_7$:Eu,Dy; 270 μL of $ZnCl_2$ (1 mol/L) for ZnS:Cu,Al and ZnS:Mn; or 270 μL of $CaCl_2$ for $CaTiO_3$:Pr into a sodium citrate buffer (0.08 mol/L) in a three-neck round-bottom flasks. The undersaturated solution was then heated to 90 °C in a silicone oil bath, and its pH was adjusted to the desired value with a sodium hydroxide (10 mol/L) solution. Reactions were initiated by introducing the bulk ML phosphor into its corresponding undersaturated solution. During the reaction, the temperature of the mixture was maintained at 90 °C, and its pH was constantly monitored with a SevenCompact S230 pH meter (Mettler Toledo, Greifensee, Switzerland). The titrant, which was composed of a sodium citrate buffer (pH 6.05; 0.08 mol/L), was added whenever the pH increased to keep the pH within ±0.1 of the targeted value. The temperature of the titrant was also maintained at 90 °C to prevent the temperature of the undersaturated etchant from changing significantly. The composition and concentration of the titrant were calculated to ensure a constant concentration of all released ions during the dissolution process, thus fulfilling the CC condition during the reaction.

Mechanoluminescence measurement in the artificial circulatory system. Tygon tubing with the inner/outer diameter of 1.59/3.18 mm was used for the artificial circulatory system as shown in **Fig. 3a**. The two ends of the tubing were immersed into a solution of ML colloidal nanocrystals (40 mg/mL) inside a 2 mL glass vial, which acted as a reservoir of the solution to prevent any air bubbles in the tubing. A peristaltic pump was used to circulate the solution with a flow rate of 11.3 mL/min. A 3D-printed tube holder was used to fix the tubing on the FUS transducer to ensure that a segment of the tubing was always at the focus of ultrasound. A 365 nm LED (M365LP1, Thorlabs, Newton, NJ) with a power density of 3.8 mW/mm^2 was used as the recharging light. FUS pulses with a central

frequency of 1.5 MHz, varied pressures, and different duration times were applied to stimulate the emission of ML colloids in the artificial circulatory system. Meanwhile, mechanoluminescence from the ultrasound focus was acquired via either a color digital EOS 5D MARK IV camera (Canon, Tokyo, Japan) or an iXon Ultra 888 electron-multiplying charge-coupled device (EMCCD) camera (Andor Technology, Belfast, United Kingdom).

Vertebrate animal subjects. Adult (20-30 g) C57BL/6J and Thy1-ChR2-YFP mice (male, 6 weeks old, Jackson Laboratory, Bar Harbor, ME) were the vertebrate animal subjects used in this study. All procedures performed on mice were approved by Stanford University's Administrative Panel on Laboratory Animal Care (APLAC). The animal care and use programs at Stanford University meet the requirements of all federal and state regulations governing the humane care and use of laboratory animals, including the USDA Animal Welfare Act, and PHS Policy on Humane Care and Use of Laboratory Animals. The laboratory animal care program at Stanford is accredited by the Association for the Assessment and Accreditation of Laboratory Animal Care (AAALAC International). Animals were group-housed on a 12 h:12 h light:dark cycle in the Stanford University's Veterinary Service Center (VSC) and fed with food and water ad libitum as appropriate.

FUS-mediated ML emission in mouse organs. C57BL/6J mice were anesthetized and transcardially perfused with 12 mL of 1× phosphate-buffered saline (PBS) followed by 3 mL of $Sr_2MgSi_2O_7$:Eu,Dy colloidal solution (40 mg/mL). Immediately afterwards, the mouse brain, liver, and kidney were collected for FUS treatment and ML imaging. Specifically, the mouse organs were placed at the ultrasound focus and charged for 10 s by a 365-nm UV LED with a power density of 0.13 mW/mm^2. 1.5 MHz FUS pulses with 30% amplitude and 20% duty cycle at a repetition rate of 1 Hz were applied 1 min after charging. The mechanoluminescence emission from the mouse organs was acquired by the EMCCD camera.

FUS-mediated optogenetic stimulation and immunohistochemical staining of the mouse brain. The Thy1-ChR2-YFP or C57BL/6J mouse was anesthetized with intraperitoneal injection of ketamine (80 mg/kg) and dexdomitor cocktail (1 mg/kg) before being placed on a heating pad (Harvard Apparatus, Holliston, MA) set to 37 ^{o}C to prevent hypothermia. Hair removal lotion (Nair, Church & Dwight) was used to remove the hair on the head and back of the mouse. Iodophor was then used to sterilize the scalp. The scalp was removed to expose the skull using surgical scissors to facilitate FUS targeting. We waited 2 h with the animal under anesthesia before proceeding to the next step to eliminate any baseline c-fos activities in the targeted brain region. The mouse head was then fixed on a head holder (SG-4N, Narishige, Tokyo, Japan), and the FUS transducer was positioned over the mouse head with ultrasound gel (Parker Aquasonic) in between.

The focus of the FUS transducer was targeted at the motor cortex (AP: +1 mm, ML: +0.5 mm, DV: -0.5 mm). Subsequently, 200 µL of $Sr_2MgSi_2O_7$:Eu,Dy colloidal solution in 1× PBS (30 mg/mL) was retro-orbitally injected, immediately before two 1.5-MHz FUS pulse train sessions (25% amplitude, 20% duty cycle, 1 Hz pulse repetition rate, 5-min session duration with a 30-s interval between the two pulse train sessions) were applied. In the meantime, a collimated beam of 365-nm light (1 mW/mm^2) from a UV-LED was applied on the depilated area of the mouse back for recharging circulating ML colloids. 90 min afterwards, the mouse was transcardially perfused with 12 mL of 1× PBS followed by 24 mL of 4% paraformaldehyde (PFA). The brain was then dissected from the skull, and post-fixed in 4% PFA for 24 h. Afterwards, the brain was transferred to 30% sucrose and was kept at 4 ^oC overnight. Coronal brain sections with 40 µm thickness were then obtained on a cryostat (Leica CM 3050S, Leica Biosystems, Wetzlar, Germany). The brain sections were washed in 1× PBS three times for 10 min each and blocked using a blocking solution consisting of 0.3% Triton X-100 and 5% donkey serum (Jackson ImmunoResearch Laboratories, West Grove, PA) in 1× PBS for 1 h at room temperature. Afterwards, the sections were incubated with rabbit anti-c-fos antibody (1:1000 dilution, ab222699, Abcam) solution containing 0.3% Triton X-100 and 5% donkey serum in 1× PBS overnight at 4 °C. After incubation, the sections were washed in 1× PBS with 0.05% Triton X-100 three times for 10 min each time at 4 °C. The sections were then incubated with donkey anti-rabbit, Alexa Fluor 594 antibody (1:500 dilution, A-21207, Invitrogen) solution containing 0.3% Triton X-100 and 5% donkey serum in 1× PBS at room temperature for 1 h. The brain sections were then washed 3 times in 1× PBS for 10 min each at 4 °C, before they were mounted on glass slides with a coverslip on top. The edges of the coverslip were sealed with transparent nail polish (Fisher Scientific), and the sections were kept in dark for 24 h before imaging. Confocal microscopic images were acquired using a LSM 980 microscope (Zeiss, Oberkochen, Germany).

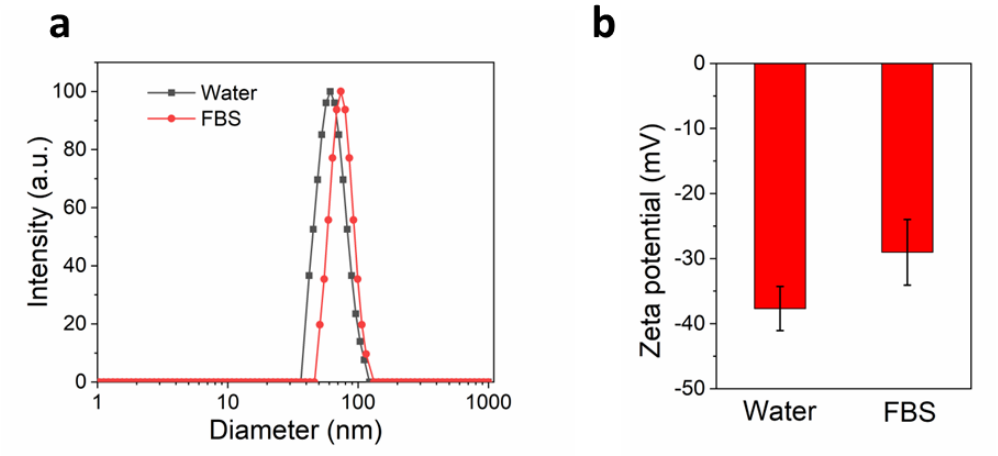

Figure S1. (**a**) Hydrodynamic diameter distribution of ML colloids of $Sr_2MgSi_2O_7$:Eu,Dy in water and FBS. (**b**) Zeta potentials of ML colloids of $Sr_2MgSi_2O_7$:Eu,Dy in water and FBS. The error bars in **b** indicate the standard deviation of three repeated measurements given by the DLS instrument.

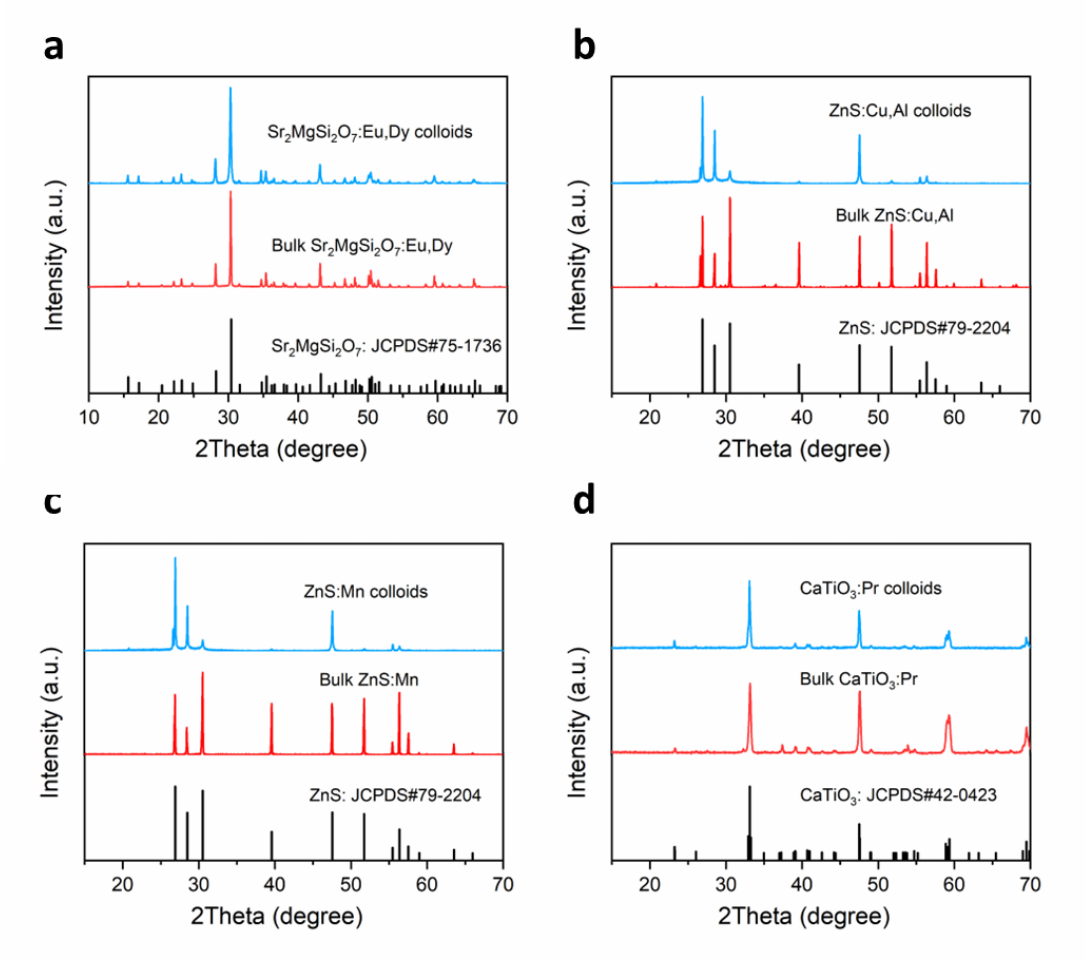

Figure S2. XRD patterns of ML colloids and their corresponding bulk precursors: (**a**) $Sr_2MgSi_2O_7$:Eu,Dy; (**b**) ZnS:Cu,Al; (**c**) ZnS:Mn; (**d**) $CaTiO_3$:Pr.

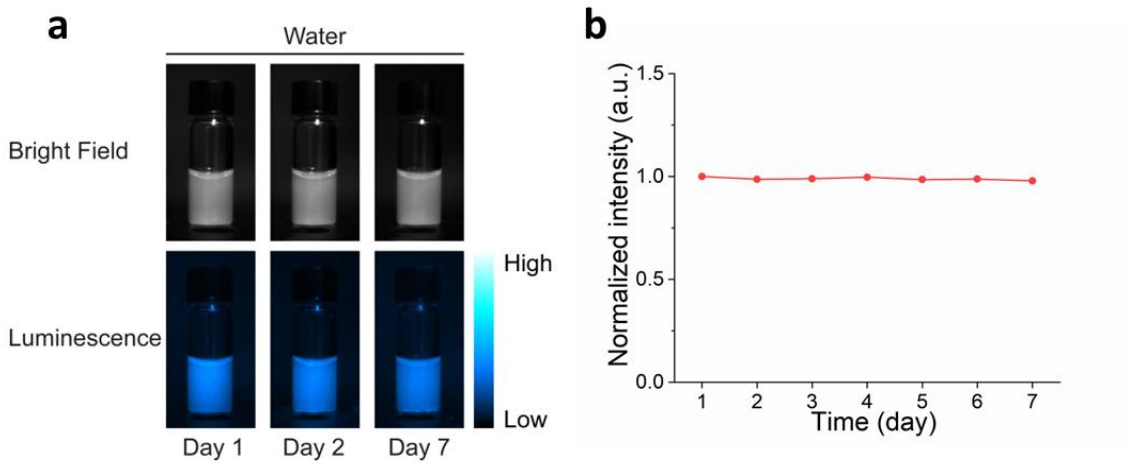

Figure S3. (**a**) Bright-field and luminescence images of PEGylated-$Sr_2MgSi_2O_7$:Eu,Dy colloids in water on Day 1, Day 2, and Day 7 after the suspension was made. (**b**) Colloidal stability of the PEGylated-$Sr_2MgSi_2O_7$:Eu,Dy colloid in water over 1 week, as evidenced by its stable luminescence intensity.

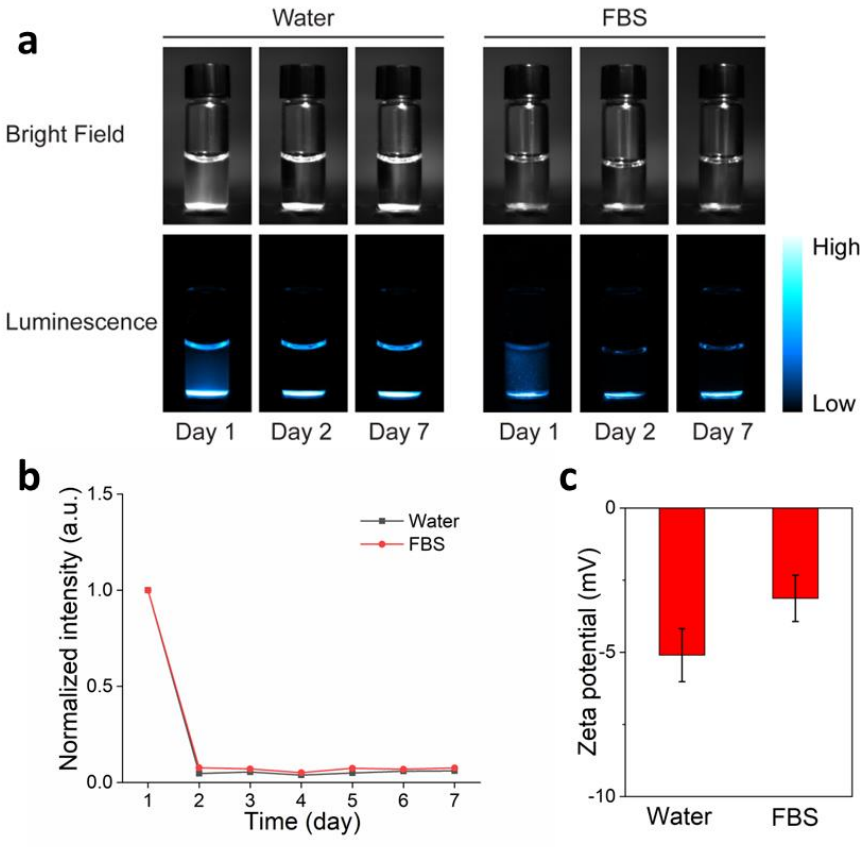

Figure S4. (**a**) Bright-field and luminescence images of $Sr_2MgSi_2O_7$:Eu,Dy bulk particles in water and FBS on Day 1, Day 2, and Day 7 after mixing. (**b**) Luminescence intensity of $Sr_2MgSi_2O_7$:Eu,Dy bulk particles in water and FBS over 1 week. (**c**) Zeta potentials of $Sr_2MgSi_2O_7$:Eu,Dy bulk particles in water and FBS.

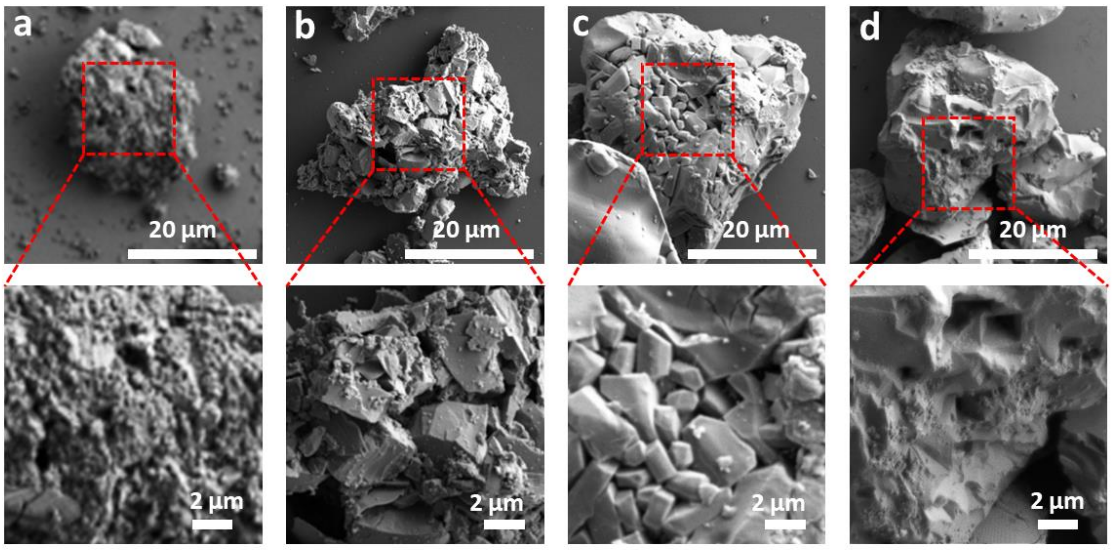

Figure S5. SEM images of bulk ML particles after the suppressed dissolution process: (**a**) $Sr_2MgSi_2O_7$:Eu,Dy; (**b**) ZnS:Cu,Al; (**c**) ZnS:Mn; (**d**) $CaTiO_3$:Pr.

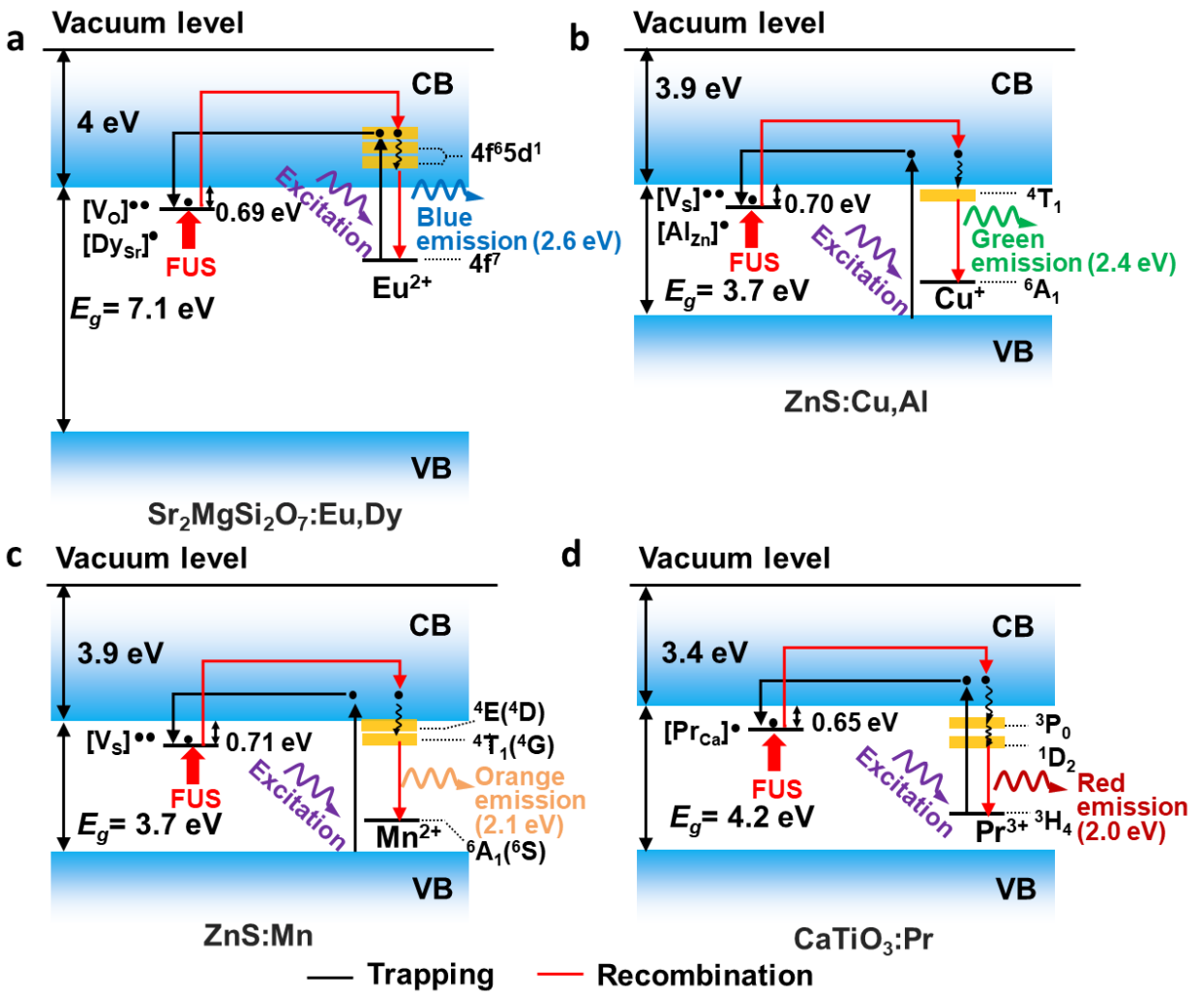

Figure S6. Schematics of ML mechanisms in trap-controlled ML materials: (**a**) SMSO; (**b**) ZnS:Cu,Al; (**c**) ZnS:Mn; (**d**) $CaTiO_3$:Pr. In each schematic, single-headed black arrows indicate the action of electrons during the excitation and trapping process, while red arrows indicate the action of electrons during the FUS-triggered detrapping and emission process. These diagrams are based on previous reports in ref. 2 (**a**), 3 (**b**), 4 (**c**), and 5 (**d**).

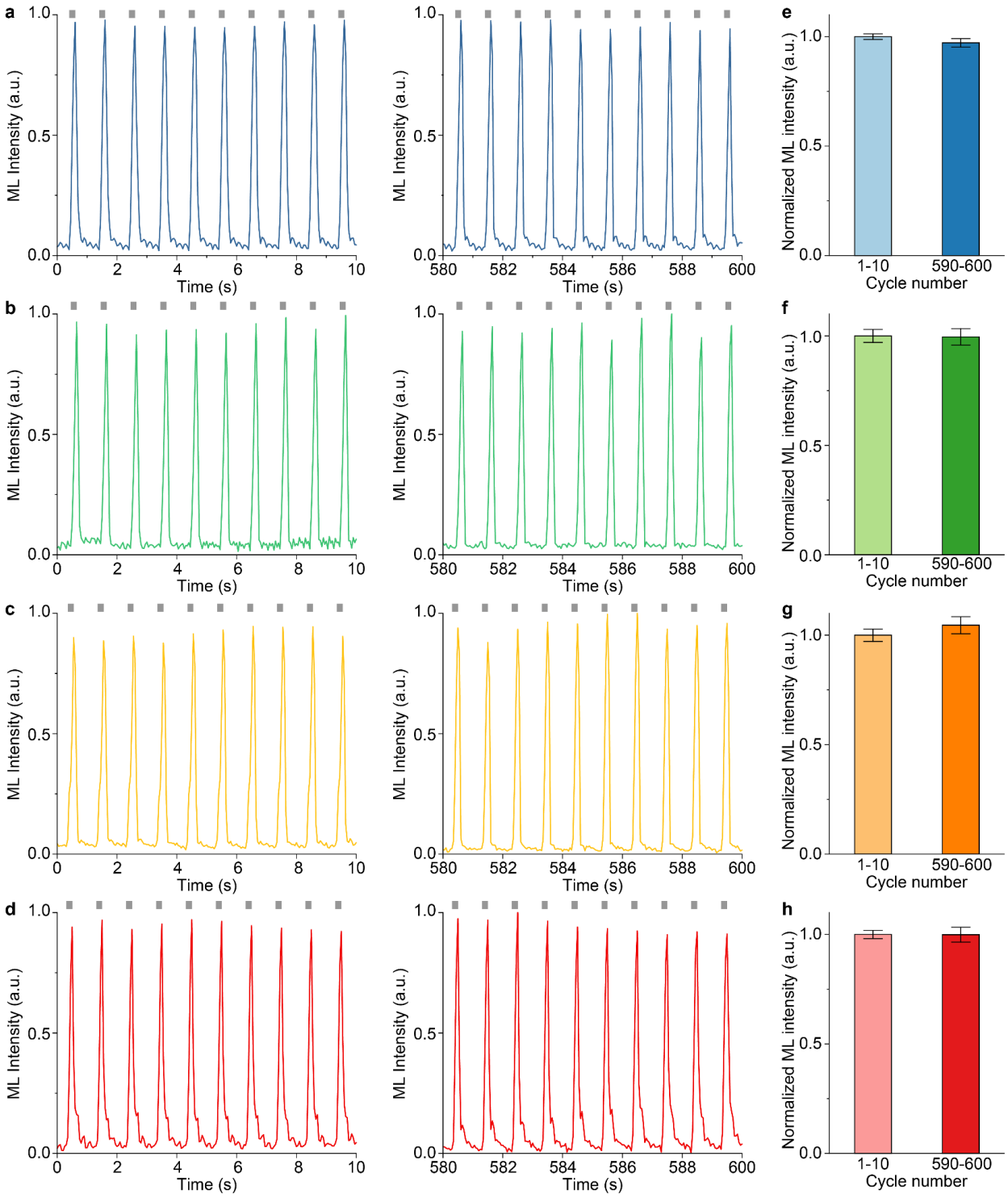

Figure S7. Rechargeability of ML colloids in the artificial circulatory system. (**a-d**) Temporal dynamics of ML intensity of $Sr_2MgSi_2O_7$:Eu,Dy (**a**), ZnS:Cu,Al (**b**), ZnS:Mn (**c**), and $CaTiO_3$:Pr colloids (**d**) in the first 10 (left) and last 10 (right) of 600 cycles in the artificial circulatory system. (**e-h**) Bar charts summarizing the ML emission intensity of $Sr_2MgSi_2O_7$:Eu,Dy (**e**), ZnS:Cu,Al (**f**), ZnS:Mn (**g**), and $CaTiO_3$:Pr colloids (**h**) in the first

10 and last 10 cycles in the artificial circulatory system. All data are presented as mean ± SD.

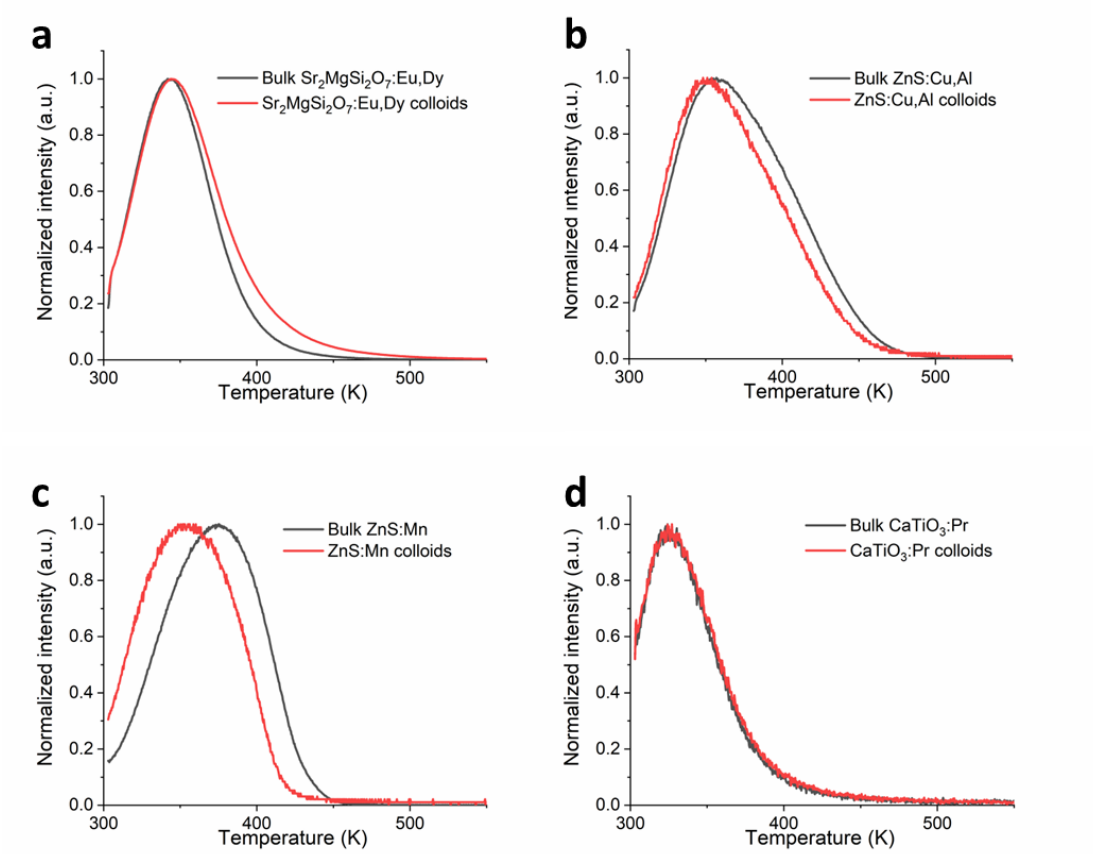

Figure S8. Thermoluminescence spectra of bulk and colloidal ML materials: (**a**) $Sr_2MgSi_2O_7$:Eu,Dy, (**b**) ZnS:Cu,Al, (**c**) ZnS:Mn, and (**d**) $CaTiO_3$:Pr.

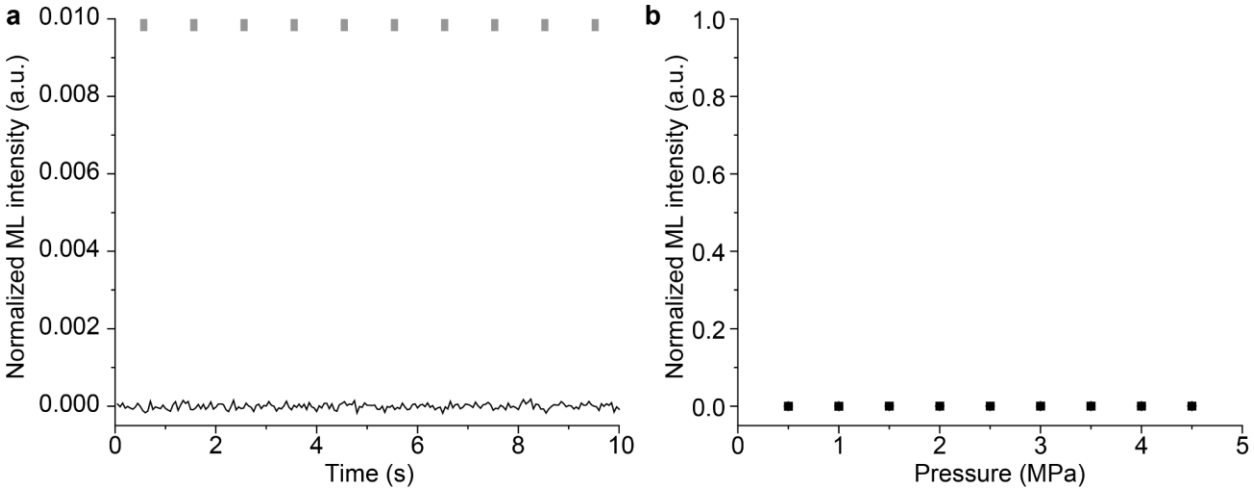

Figure S9. The carrier medium without ML colloids does not produce mechanoluminescence under ultrasound. (**a**) A representative time trace of light intensity measurement from the carrier medium alone in the artificial circulatory system under repeated FUS pulses, the latter of which are indicated by gray ticks. (**b**) Light emission intensity from the carrier medium as a function of FUS peak pressure. The data are presented as mean ± SD of 10 independent measurements. All intensities are normalized against the ML intensity of $Sr_2MgSi_2O_7$:Eu,Dy colloids under a hydrodynamic pressure of 4.5 MPa in **Fig. 6a**.

Supplementary References

(1) Tang, R.; Nancollas, G. H.; Orme, C. A. Mechanism of Dissolution of Sparingly Soluble Electrolytes. *J. Am. Chem. Soc.* **2001**, *123* (23), 5437–5443.

(2) Xiao, L.; Zhou, J.; Liu, G.; Wang, L. Luminescent Properties of R^+ Doped $Sr_2MgSi_2O_7$: Eu^{2+}, Dy^{3+} (R = Li^+, Ag^+) Phosphors. *J. Alloys Compd*. **2017**, *712*, 24–29.

(3) Wong, M.-C.; Chen, L.; Tsang, M.-K.; Zhang, Y.; Hao, J. Magnetic-Induced Luminescence from Flexible Composite Laminates by Coupling Magnetic Field to Piezophotonic Effect. *Adv. Mater.* **2015**, *27* (30), 4488–4495.

(4) Zhou, H.; Du, Y.; Wu, C.; Jiang, Y.; Wang, F.; Zhang, J.; Wang, Z. Understanding the Mechanoluminescent Mechanisms of Manganese Doped Zinc Sulfide Based on Load Effects. *J. Lumin.* **2018**, *203*, 683–688.

(5) Zhang, J-C; Wan, Y.; Xin, X.; Han, W. P.; Zhang, H. D. Elastico-Mechanoluminescent Enhancement with Gd^{3+} Codoping in Diphase (Ba,Ca)TiO_3:Pr^{3+}. *Opt. Mater.* **2014**, *4* (11), 2300-2309.